

Uptake selectivity of Methanesulfonic Acid (MSA) on fine particles over polynya regions of the Ross Sea, Antarctica

Jinpei Yan^{*1,2}, Jinyoung Jung³, Miming Zhang^{1,2}, Federico Bianchi⁴, Yee Jun Tham⁴, Suqing Xu^{1,2},
Qi Lin^{1,2}, Shuhui Zhao^{1,2}, Lei Li⁵, Liqi Chen^{1,2}

1 Key Laboratory of Global Change and Marine-Atmospheric Chemistry, MNR, Xiamen 361005, China;

2 Third Institute of Oceanography, Ministry of Natural Resources, Xiamen 361005, China;

3 Korea Polar Research Institute, 26 Songdomirae-ro, Yeonsu-gu, Incheon 21990, Republic of Korea;

4 Institute for Atmospheric and Earth System Research; University of Helsinki, 00014, Finland;

5 Institute of Mass Spectrometer and Atmospheric Environment, Jinan University, Guangzhou 510632, China

Abstract: The uptake of methanesulfonic acid (MSA) on existing particles is a major route of the particulate MSA formation, however, MSA uptake on different particles is still lack in knowledge. Characteristics of MSA uptake on different aerosol particles were investigated in polynya (an area of open sea water surrounded by ice) regions of the Ross Sea, Antarctica. Particulate MSA mass concentration, as well as aerosol population and size distribution, were observed simultaneously for the first time to access the uptake of MSA on different particles. The results show that MSA mass concentration does not always reflect MSA particle population in the marine atmosphere. MSA uptake on aerosol particle increases the particle size and changes aerosol chemical composition, but does not increase the particle population. The uptake rate of MSA on particle is significantly influenced by aerosol chemical properties. Sea salt particles are beneficial for MSA uptake, as MSA-Na and MSA-Mg particles are abundant in the Na and Mg particles, accounting for 0.43 ± 0.21 and 0.41 ± 0.20 of the total Na and Mg particles, respectively. However, acidic and hydrophobic particles suppress the uptake of MSA, as MSA-EC and MSA-SO₄²⁻ particles account for only 0.24 ± 0.68 and 0.26 ± 0.47 of the total EC and SO₄²⁻ particles, respectively. The results extend the knowledge of the formation and environmental behavior of MSA in the marine atmosphere.

Keywords: Methanesulfonic acid (MSA); nss-SO₄²⁻; aerosol; climate change; Antarctica

1. Introduction

*Corresponding author. Tel.: +86 592 2195370; Fax: +86 592 2195280, E-mail address: jpyan@tio.org.cn; Address: No.178 Daxue Road, Siming district Xiamen, Third Institute of Oceanography, MNR, 361005, P R China.

25 Methanesulfonic acid (MSA) and non-sea-salt-sulfate (nss-SO_4^{2-}), derived from the oxidation
26 of dimethyl sulfide (DMS), are important sources of cloud condensation nuclei (CCN) in the
27 marine boundary layer (Chang et al., 2011; Ghahremaninezhad et al., 2016). Different from
28 nss-SO_4^{2-} , MSA is exclusively from the oxidation of DMS in the atmosphere (Sorooshian et al.,
29 2007). Thus, MSA is expected as a useful marker for the deconvolution of sulfate from marine
30 biogenic and non biogenic sources (Legrand et al., 1998). The ratio of MSA to nss-SO_4^{2-} is often
31 used to assess the DMS oxidation routes and the contributions of biogenic sulfur to other sulfur
32 sources (Sorooshian et al., 2007; Wang et al., 2014). DMS oxidation routes, as well as the
33 products of MSA and nss-SO_4^{2-} , have been investigated previously in the marine atmosphere
34 (Preunkert et al., 2008; Kloster et al., 2006).

35 Generally, particulate MSA is generated from the reactive uptake of DMS and condensation of
36 gaseous MSA on aerosol particles (Davis et al., 1998; Barnes et al., 2006). A recent study has
37 shown that MSA can increase sulfate cluster formation rate by up to one order of magnitude,
38 increasing the stability of the clusters (Bork et al., 2014). However, previous studies have shown
39 that SO_4^{2-} is more effective at new particle formation (NPF) than MSA, while MSA is more
40 likely to condense onto existing particles (Hayashida et al., 2017). Although the reactive uptake
41 of MSA on fine particle has been demonstrated in the previous studies (Sorooshian et al., 2007;
42 Bates et al., 1992), the influence of aerosol characteristics on MSA uptake is not present.

43 The chemical components and sources of aerosol particles in the marine atmosphere are very
44 complicated (Weller et al., 2018). Filtered sample methods are often used in previous studies (Jung
45 et al., 2014; Preunkert et al., 2007; Read et al., 2008), with a long sampling interval to
46 accommodate the detection limit of the instrument (Preunkert et al., 2007; Zhang et al., 2015). It is,
47 therefore, difficult to clarify how MSA mixes with other aerosol species, using bulk aerosol
48 sampling methods, as only mean aerosol chemical components are obtained during the sampling
49 period (Bates et al., 1992; Chen et al., 2012). On-line aerosol mass spectrometry has been used to
50 characterize the aerosol chemical species and sizes with high-time-resolution (Yan et al., 2018;
51 Healy et al., 2010), allowing the determination of particle mixing states and sources. Although a
52 few studies have shown that MSA is often associated with Mg in aerosol particles, probably due to
53 marine biogenic activity (Casillas-Iuarte et al., 2010), studies of the interactions between MSA

54 and other aerosol species are still rare. Theoretical and laboratory studies have attempted to
55 explain these observations and determine in which way MSA enters aerosol particle (Bork et al.,
56 2014). However, the relative likelihood of MSA uptake on different particles remains uncertain.

57 In this study, we examined the uptake characteristics of MSA on different particles over polynya
58 (an area of open sea water surrounded by ice) regions in the Ross Sea (RS), Antarctica, based on
59 high-time-resolution observations. MSA mass concentrations and particle populations, as well as
60 aerosol compositions and size distributions, were measured simultaneously for the first time in the
61 RS using an in-situ gas and aerosol compositions (IGAC) and a single particle aerosol mass
62 spectrometer (SPAMS) monitoring instrument. Observations were carried out in two different
63 seasons, the early December with intense sea ice coverage and in the mid-January to February
64 with sea ice free in the RS.

65 **2. Experiment methods and observation regions**

66 The observations were carried out on-board of R/V “Xuelong”, covering a large region of the
67 RS, Antarctica (50°S to 78°S, 160°E to 185°E) (Fig. S1) with different sea ice concentrations. The
68 leg I was carried out from December 2 to 20, 2017. The sea surfaces were covered with intense
69 sea ice in the RS during this period (Fig. S2a). However, when we arrived back in the RS (leg II,
70 from January 13 to February 14, 2018), the sea ice had almost melted in the RS (Fig. S2b).

71 **2.1 Observation instruments and sampling inlet**

72 An in-situ gas and aerosol compositions monitoring system (IGAC, Model S-611, Machine
73 Shop, Fortelice International Co., Ltd., Taiwan; <http://www.machine-shop.com.tw/>), and a single
74 particle aerosol mass spectrometer (SPAMS, Hexin Analysis Instrument Co., Ltd.) were used to
75 determine aerosol water-soluble ion species, particle size distributions and chemical compositions,
76 respectively (Fig. S3). The sampling inlet connecting to the monitoring instruments was fixed to a
77 mast 20 meters above the sea surface to minimize the impact of self-contaminations of the vessel.

78 Wind speeds and directions were also monitored during the cruise. The observation periods in
79 which self-contaminations impacted the measurement have been excluded based on the high-time-
80 resolution observation data. A total suspended particulate (TSP) sampling inlet was positioned at
81 the top of the mast. Conductive silicon tubing with an inner diameter of 1.0 cm was used to make
82 the connection to all instruments.

83 **2.2 Aerosol water-soluble ion species**

84 Gases and aerosol water-soluble ion species were determined using a semi-continuous IGAC
85 monitor. A PM₁₀ cyclone was conducted for the IGAC sampling. Hence, the measurement particle
86 size is ~10µm of the IGAC in this study. Gases and aerosols are separated and streamed into a
87 liquid effluent for on-line chemical analysis at an hourly temporal resolution (Young et al., 2016;
88 Liu et al., 2017). The analytical design and methodology for the determination of gases and
89 aerosol water-soluble ions have been described in detail by Tao (2018) and Tian (2017). Fine
90 particles are firstly enlarged by vapor condensation and subsequently accelerated through a
91 conical-shaped impaction nozzle and collected on the impaction plate. The samples are then
92 subsequently analyzed for anions and cations by an on-line ion chromatography (IC) system
93 (DionexICS-3000). The injection loop size is 500 µL for both anions and cations. Six to eight
94 concentrations of standard solutions are selected for calibration, depending on the target
95 concentration, in which the R² was above 0.997 (Fig. S4). The detection limits for MSA⁻, SO₄²⁻,
96 Na⁺, and Cl⁻ are 0.09, 0.12, 0.03, and 0.03 µg/L (aqueous solution), respectively.

97 **2.3 Aerosol size distribution and chemical compositions**

98 The detection method for fine particles (0.1-2.0 µm) using a SPAMS has been described in
99 detail by Li (Li et al., 2011; Li et al., 2014). Particles are introduced into the vacuum system
100 through a critical orifice, then focused and accelerated to form a particle beam with specific

101 velocity. The particle beam passes through two continuous diode Nd: YAG lasers (532 nm), where
102 the scattered light is detected by two Photomultiplier Tubes (PMTs). The velocity of a single
103 particle is then determined and converted into its aerodynamic diameter. The individual particle is
104 ionized with a 266 nm Nd: YAG laser to produce positive and negative ions. The fragment ions are
105 analyzed using a bipolar time-of-flight mass spectrometer. The power density of the ionization
106 laser is kept at $1.56 \times 10^8 \text{ W.cm}^{-2}$.

107 The particle size data and mass spectra are analyzed using the YAADA software toolkit
108 (<http://www.yaada.org/>) (Allen 2005). An adaptive resonance theory based neural network
109 algorithm (ART-2a) is applied to cluster individual particles into separate groups based on the
110 presence and intensity of ion peaks in the single particle mass spectrum (Song et al., 1999), with a
111 vigilance factor of 0.65, a learning rate of 0.05, and a maximum of 20 iterations.

112 **2.4 Metrological data**

113 Meteorological parameters such as temperature, humidity, wind speed, and direction were
114 measured continuously using an automated meteorological station deployed in the R/V "Xuelong",
115 which was located on the top deck of the vessel.

116 **2.5 Satellite data of sea ice and chlorophyll-a**

117 In this study, we used remote sensing data to show the spatial and temporal distribution of
118 chlorophyll and sea ice concentrations in the RS. To reduce the impact of cloud and swath limits,
119 we chose the 8-day datasets for the remote sensing of chlorophyll-a from MODIS-Aqua
120 (<http://oceancolor.gsfc.nasa.gov>) with a spatial resolution of 4 km. We used the sea ice
121 concentration data from the daily 3.125-km AMSR2 dataset (Spreen et al., 2008) (available at
122 <https://seaice.uni-bremen.de>). Each grid of the gridded datasets with a sea ice concentration less
123 than or equal to 15 % was regarded as comprising all water (Cavalieri et al., 2003). The time series
124 of the total regional mean value in the study region was then plotted.

125 **3. Results and discussion**

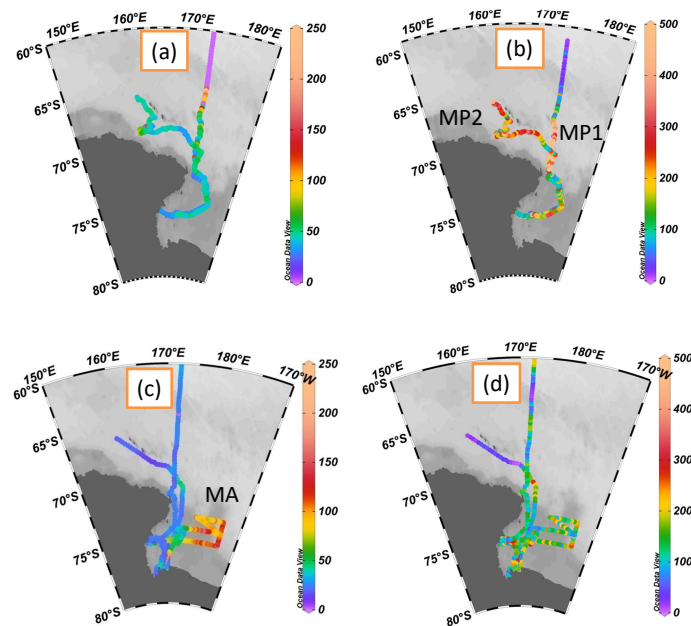
126 **3.1. Spatial distributions of MSA mass concentration and particle population**

127 MSA mass concentrations were measured continuously in the RS. The spatial distributions of
128 MSA mass concentrations and particle populations in Fig. 1 are created with Ocean Data View
129 (Schlitzer 2015; Schlitzer et al., 2002). MSA concentrations ranged from 14.6 to 210.8 ng.m⁻³,
130 with an average of 43.8±22.1 ng.m⁻³ during leg I (Fig.1a), consisting with summertime MSA
131 levels recorded at Halley station (75°39'S, with an average of 35.3 ng.m⁻³) and Dumont d'Urville
132 station (66°40'S, with an average of 49 ng.m⁻³) (Minikin et al., 1998), but lower than those
133 reported at Palmer station (64°77' S, with an average of 122 ng.m⁻³) (Savoie et al., 1993). The
134 highest MSA levels occurred at the region (64° - 67° S), with an maximum value of 210.8 ng.m⁻³
135 (Fig. 1a), consisting with the previous observation results obtained from the Southern Ocean (60 -
136 70° S; maximum MSA level of 260 ng.m⁻³) (Chen et al., 2012). In this study, elevated MSA levels
137 were associated with the dynamic sea ice edge at ~64° S, as sea ice starts to melt in the early
138 December (Fig. S2a and Fig. S2c). The release of iron (De Baar et al., 1995; Wang et al., 2014)
139 and algae (Lizotte et al., 2001; Loose et al., 2011) from sea ice increase phytoplankton numbers
140 (Taylor et al., 2013), resulting in the increase of DMS generation and emission (Hayashida et al.,
141 2017). This, in turn, increases MSA levels due to the oxidation of DMS in the atmosphere.

142 MSA particle populations (0.1 - 2.5 µm) were determined simultaneously by SPAMS during the
143 cruise (Fig. 1b). The highest average hourly MSA particle population (507 ± 189) occurred at
144 MP1 (high MSA population, 68° - 72°S, 172°E) near the Antarctic continent, followed by MP2
145 (high MSA population, 65° - 68°S, 160° - 170° E), with an average particle population of 344 ±
146 334. High MSA particle populations were associated with high wind speeds in these regions (MP1
147 8.06 ± 1.86m/s, MP2 15.76 ± 3.93m/s, Fig. 2).

148 The MSA mass concentrations ranged from 11.4 - 165.4 ng•m⁻³ (with an average of 38.8 ± 27.5

149 $\text{ng}\cdot\text{m}^{-3}$) during leg II, and the MSA particle populations ranged from 3 - 1666 (with an average of
150 168 ± 172 , [Fig. 1c and 1d](#)). Similar variations of MSA particle population and total particle
151 population were present ([Fig. 2](#)). The relationship between MSA particle population and total
152 particle population will be further discussed in section 3.2. Extremely high MSA mass
153 concentrations, with an average of $100.3 \pm 18.6 \text{ ng}\cdot\text{m}^{-3}$, were observed in the MA region (high
154 MSA mass, $170.2^\circ - 177.4^\circ\text{E}$, $68.2^\circ - 77.8^\circ\text{S}$), but high MSA particle populations were not present
155 in this region (with an average of 171 ± 159). High MSA particle populations with low MSA
156 concentrations occurred at MP1 and MP2 ([Fig. 1a and 1b](#)). It indicates that MSA mass
157 concentrations did not always reflect the MSA particle populations in the marine atmosphere.
158 Generally, the uptake of MSA on aerosol surface ([Read et al., 2008](#)) only changes the aerosol size
159 and chemical composition, without varying their populations. Hence, the MSA particle population
160 is mainly associated with the aerosol number concentration in the atmosphere, as more particles
161 are provided for the uptake of MSA in high particle number concentration. Though high levels of
162 MSA may also increase the MSA population, high MSA mass concentrations with low MSA
163 populations are observed in this study. This phenomenon occurs when low existing particle
164 populations and high MSA mass concentrations are present in the marine atmosphere.



165

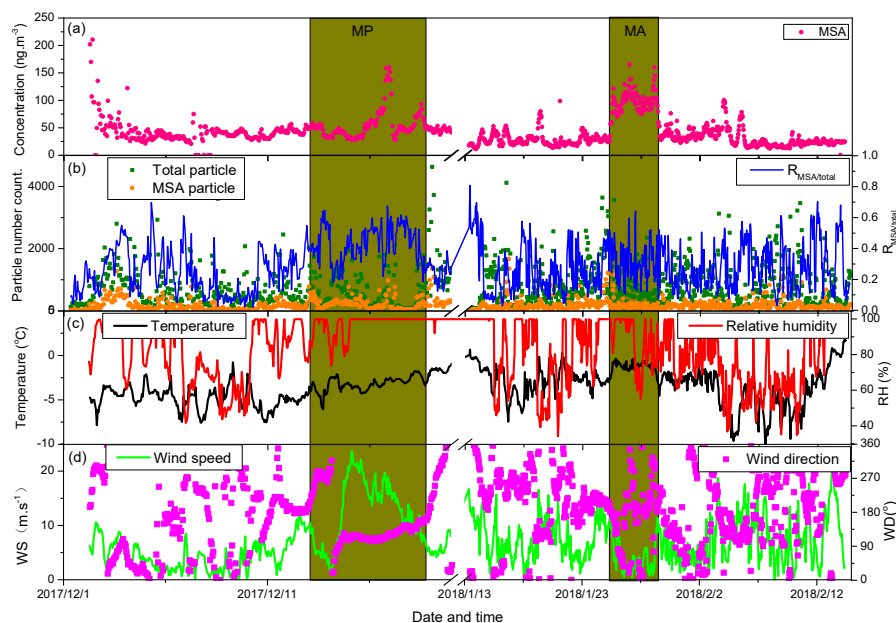
166 Fig.1 Spatial distribution of MSA mass concentrations and particle populations, (a) MSA mass
 167 concentrations during leg I (ng.m^{-3}); (b) MSA particle populations during leg I;
 168 (c) MSA mass concentrations during leg II (ng.m^{-3}) and (d) MSA particle populations during leg II.

169 **3.2. Linkage between MSA concentration and particle population**

170 To verify the relationship between MSA mass concentration and particle population, the
 171 temporal distributions of MSA mass concentration and particle number are illustrated in Fig. 2.
 172 Variations of MSA mass concentrations were not always associated with the MSA particle
 173 populations during the observation periods (Fig. 2a and 2b). We did not find an obvious
 174 correlation between MSA particle population and MSA mass concentration (Fig. S5a), indicating
 175 that the major factors regulating MSA mass concentration and MSA particle population were
 176 different. High MSA particle populations often occurred in conjunction with high wind speeds
 177 (Fig. 2b and 2d), while high MSA mass concentrations were not always observed at high wind
 178 speed regions, such as extremely high MSA mass concentrations with low wind speeds were
 179 present at MA (Fig. 2a, 2b and 2d).

180 MSA mass concentrations are determined by the oxidation of DMS, derived from marine
 181 phytoplankton activity (Davis et al., 1998; Barnes et al., 2006; Read et al., 2008), but MSA
 182 particle populations are mainly associated with the uptake of MSA on existing particles. High
 183 existing particle populations lead to high MSA particle populations, as the formation of particulate
 184 MSA often occurs on the surface of existing particle (Read et al., 2008). In this study, the
 185 variation of MSA particle population was consistent with the variation of total particle population

186 during the observation period (Fig. 2b). A positive correlation between MSA particle population
 187 and total particle population was present (slope=0.19, $r^2=0.65$, $n=1195$, Fig. S5b). The ratio of
 188 MSA particle population to total particle population ($R_{\text{MSA/total}}$) concentrated on the range of 0.2 -
 189 0.5, with an average of 0.29 ± 0.15 (Fig. 2b).



190
 191 Fig. 2 Relationship between MSA mass concentration and MSA particle population in the context
 192 of various environmental factors. (a) Time series of MSA mass concentrations; (b) Time series of
 193 MSA particle population, total particle population and the ratio of MSA particle population and
 194 total particle population; (c) Time series of temperature and relative humidity (RH); and (d) Time
 195 series of wind speeds and direction.

196 3.3. Signatures of MSA particle types

197 During leg I, 332438 single particles with positive and negative mass spectra were obtained,
 198 while 603098 single particles with positive and negative mass spectra were obtained during leg II.
 199 Fine particles were classified as eight types, such as Na, Mg, SO_4^{2-} , K, EC, OC, NO_x^- and MSA,
 200 using the ART-2a algorithm (Song et al., 1999) during the cruise (Fig. S6). MSA particles
 201 accounted for 27.69 % and 22.08 % of the total particles during leg I and leg II, respectively. To
 202 investigate the interaction between MSA and other species, MSA particles were further classified
 203 into seven sub-types, including MSA-Na, MSA-Mg, MSA-SO_4^{2-} , MSA-K, MSA-EC, MSA-OC,
 204 and MSA-NO_x^- .

205 3.3.1 MSA-Na particles

206 Sodium, which is often associated with sea salt particles in the marine atmosphere (Teinila et
207 al., 2014), is an important component of atmospheric aerosols in ocean regions (Yan et al., 2018).
208 Fig. 3a illustrates the average mass spectra of MSA-Na particles during leg I and leg II. Strong
209 Na^+ peaks with weak K^+ , Ca^+ , and Na_2Cl^+ peaks were observed in the positive spectrum, while
210 strong NaCl_2^- and MSA^- peaks with low Cl^- , HSO_4^- , NO_3^- , and O^- peaks were present in the
211 negative spectrum. Similar average mass spectra for MSA-Na particles were observed during leg I
212 and leg II, even though the two measurements were carried out under different circumstances.
213 MSA-Na particles were the most dominant type of MSA particles, accounting for more than 30 %
214 of total MSA particles (Fig. 4d).

215 3.3.2 MSA-Mg particles

216 Mg is another common component in ocean-derived particles, hence, such particles are often
217 classified as sea salt particles in the marine atmosphere. However, some previous studies have
218 shown that the chemical properties of Mg particles observed in marine environment are distinct
219 from those of sea salt particles (Gaston et al., 2011). In this study, the mass spectral characteristics
220 of MSA-Mg type particles included strong MSA^- and Mg peaks (Fig. 3b). In sea salt particles, the
221 dominant peak was typically Na^+ rather than Mg^+ (Fig. 3a) due to the higher concentration of Na^+
222 in seawater (Guazzotti et al., 2001). Similar with MSA-Na type particles, strong Na^+ and NaCl_2^-
223 peaks with weak Cl^- , NO_3^- , K^+ , and Ca^+ peaks were observed in the mass spectra, indicating that
224 MSA-Mg type particles were also derived from sea salt particles. Strong positive correlation
225 ($r^2=0.95$) between MSA-Na and MSA-Mg was present in this study (Fig. S7), indicating that these
226 two types of particles were derived from the same sources. However, the abundance of Mg^+

227 fragment ion relative to Na^+ fragment ion in MSA-Mg type particles was different from MSA-Na
228 particles, indicating that MSA-Mg particles were also affected by other sources. Studies have
229 shown that Mg particles are correlated strongly with atmospheric DMS ($r^2=0.76$) (Gaston et al.,
230 2011), indicating that Mg particles are also impacted by marine biological materials, such as cell
231 debris or fragments, viruses, bacteria, or the organics released by lysed cells (Casillas-Ituarte et al.,
232 2010; Gaston et al., 2011). Hence, MSA-Mg type particles were associated with both sea salt
233 particles and biological emissions in this study.

234 3.3.3 MSA- SO_4^{2-} particles

235 SO_4^{2-} particles are derived from different sources, such as sea salt aerosols, anthropogenic
236 emissions, marine biogenic and volcanic sources (Legrand et al., 1998). Strong signals, peeking at
237 m/z -97 HSO_4^- and m/z -95 MSA^- , were present in the negative spectrum (seen in Fig. 3c),
238 consisting with previous studies with intense signals of HSO_4^- and MSA^- occurred at m/z -97 and
239 m/z -95 (Gaston et al., 2011; Silva et al., 2000). Peaks of K^+ , Na^+ , Al^+ , and Fe^+ were present in the
240 positive mass spectrum and NaCl_2^- , NO_3^- , C_4H^- and C_2H_2^- peaks were present in the negative mass
241 spectrum, suggesting that MSA- SO_4^{2-} particles were associated with different sources. This can be
242 further demonstrated by the size distribution of MSA- SO_4^{2-} particles (Fig. 5c and 5d), as
243 MSA- SO_4^{2-} particles were found in both submicron particles (0.1-1.0 μm) and coarse particles
244 (1.0~2.0 μm).

245 3.3.4 MSA-K particles

246 The positive mass spectrum of the MSA-K particles was dominated by a strong K^+ peak with
247 weak Na^+ , C_2H_3^+ and C_3H_7^+ peaks (Fig. 3d). Strong HSO_4^- and MSA^- signals were present in the
248 negative mass spectrum. Abundance of organic fragment ions were observed in the mass spectra

249 of MSA-K particles. K is often expected as a marker of biomass-burning source in continental
250 areas (Yan et al., 2018). But K is also derived from other sources, such as coal combustion and
251 biological materials. The mass spectra of MSA-K particles observed in this study were very
252 different from the mass spectra of K particles observed from biomass burning, indicating that K
253 particles were not associated with the biomass burning here.

254 3.3.5 MSA-OC particles

255 OC particles are often associated with anthropogenic sources, such as vehicle and coal
256 combustion (Silva et al., 2000; Stiaras et al., 2008), marine biogenic sources (Quinn et al., 2014)
257 and secondary sources (photochemical reaction from their precursor organic gases) (Horne et al.,
258 2018). The positive and negative mass spectra of MSA-OC were dominated by C_xH_y ion peaks
259 (i.e., $C_2H_3^+$, C_3H^+ , $C_3H_3^+$, $C_3H_4^+$, and $C_3H_7^+$; Fig. 3e). Strong signals of HSO_4^- and MSA^- fragment
260 ions were also present in the negative spectrum, while weak signals of Na^+ and Cl^- were observed
261 in the positive mass spectrum (Fig. 3e).

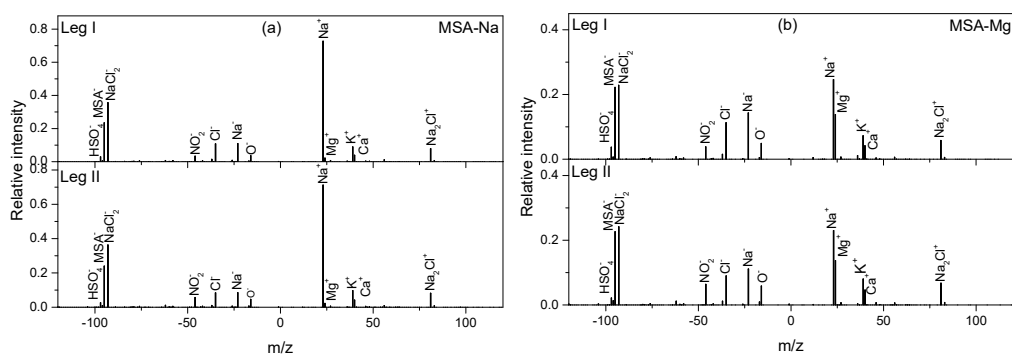
262 3.3.6 MSA-EC particles

263 EC particles are often associated with primary emissions; that is, the incomplete combustion
264 of carbon-containing materials (Murphy et al., 2009). In this study, MSA-EC particles were
265 characterized by strong peaks of C_n^- (C_4^- , C_3^- and C_2^-) in the negative spectrum, while the positive
266 mass spectrum was dominated by Ca^+ ions (Fig. 3f). EC particles are often associated with ship
267 emissions in the ocean atmosphere (Yan et al., 2018). Compare with the average mass spectra of
268 MSA-OC particles, the abundances of MSA^- and HSO_4^- fragment ions were lower in MSA-EC
269 particles, indicating that the uptake of MSA on EC particles may be more difficult than the uptake
270 of MSA on OC particles. Similar with the mass spectra of MSA-OC particles, a few fragments of

271 Na^+ and Cl^- were observed in the MSA-EC mass spectra, suggesting that MSA-OC and MSA-EC
272 particles rarely mixed with sea salt particles.

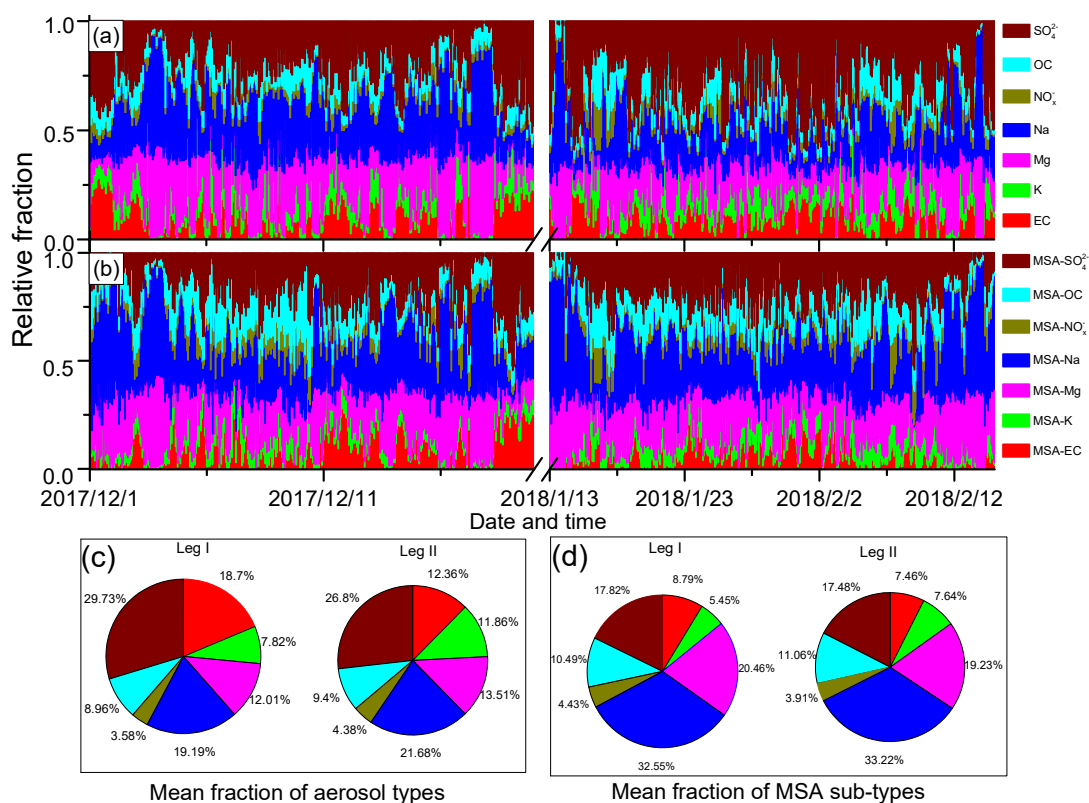
273 3.3.7 MSA- NO_x^- particles

274 The negative spectrum of MSA- NO_x^- particle was dominated by strong peaks of MSA^- , NO_2^- ,
275 and NO_3^- , with weak C_xH_y^- , O^- , and Cl^- peaks (Fig. 3g). Strong Na^+ , $(\text{C}_3\text{H}_3^+)/\text{K}^+$, and $(\text{C}_3\text{H}_4^+)/\text{Ca}^+$
276 peaks with weak Na_2Cl^+ and CaO^+ peaks were observed in the positive spectrum. Sea salt particles
277 react easily with atmospheric HNO_3 to form nitrate and hydrogen chloride (Adachi et al., 2015).
278 The abundance of Na^+ , Cl^- , and NaCl_2^- ions in the mass spectra of MSA- NO_x^- particles
279 demonstrated these particles were formed by the interaction between sea salt particles and NO_x^- in
280 the marine atmosphere. Generally, NO_x^- components (NO_2^- and NO_3^-) are produced from their
281 precursor gases NO_2 , N_2O and NO , mainly deriving from natural sources in the SO (Wolff, 1995)
282 and also impacted by the human activities in the coastal Antarctic regions (Mazzera et al., 2001).
283 High concentrations of NO_x^- are often found in urban atmospheric aerosols (Yan et al., 2015).
284 However, the concentrations of NO_x^- were extremely low during the whole cruise (Fig. 4),
285 indicating that NO_x^- was associated with the marine sources in this study.



286

300 The average fractions of the MSA sub-type particles differed considerably from the average
301 fractions of their corresponding particle types (Fig. 4c and 4d). SO_4^{2-} particles accounted for 26.8%
302 of the total particles (Fig. 4c). However, MSA- SO_4^{2-} particles accounted for only about 17.8% of
303 the total MSA particles (Fig. 4d). Similarly, the relative abundances of MSA-EC and MSA-K with
304 respect to total MSA particles were lower than those of EC and K with respect to the total particles.
305 In contrast, MSA-Na particles were the most abundant MSA particles, accounting for more than
306 32.55% of the total MSA particles (Fig. 4d), while Na particles accounted for only 21.68% of the
307 total particles (Fig. 4c). Similar patterns were observed for Mg and OC particles. MSA-Mg and
308 MSA-OC particles were more abundant in the MSA particles than Mg and OC particles in the
309 total particles (Fig. 4d). These results indicate that the uptake of MSA on Na and Mg particles
310 were more effective than the uptake of MSA on EC and SO_4^{2-} particles. Note that observations
311 during leg I and leg II were conducted under different circumstances, as high concentrations of sea
312 ice were present during leg I (Fig. S2a) but sea ice free occurs during leg II (Fig. S2b). Despite
313 different conditions were present during leg I and leg II, the relative fractions of MSA sub-type
314 particles remain similar, confirming the uptake selectivity of MSA occurred on different particles.



315

316 Fig. 4 Relative fractions of different particle types during leg I and leg II. (a) Relative fractions of
 317 different particle types; (b) Relative fractions of MSA sub-type particles; (c) Average fractions of
 318 different particle types during leg I and leg II; and (d) Average fractions of MSA sub-type particles
 319 during leg I and leg II.

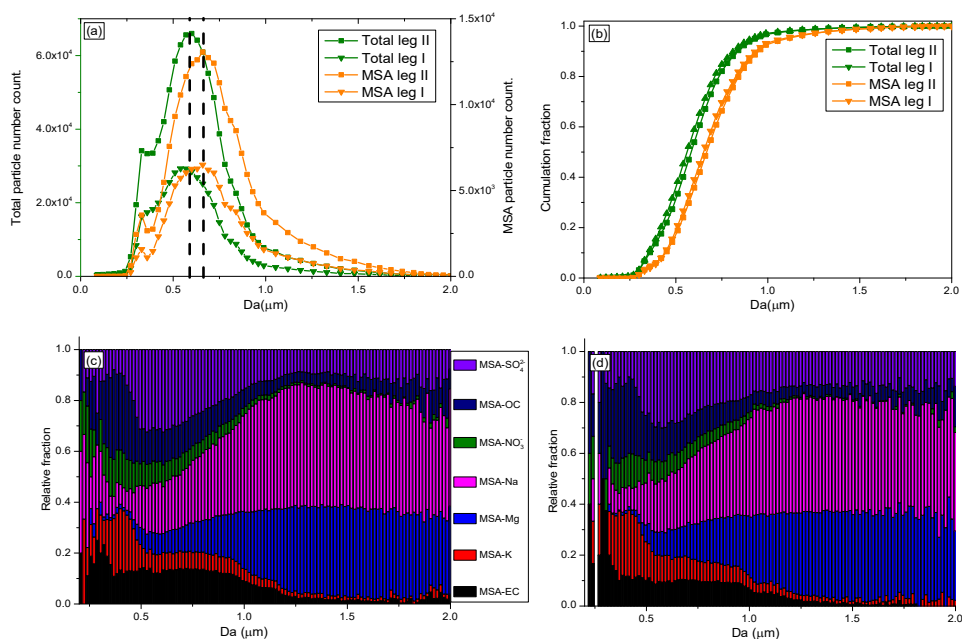
320 As discussed above, relative fractions of MSA sub-type particles were different from their
 321 corresponding particles. The contributions of MSA-Na and MSA-Mg to the total MSA particles
 322 were improved significantly, while the contribution of MSA- SO_4^{2-} declined. Fig. S8 illustrates the
 323 mean fractions of MSA sub-type particles to the total particle population. Similar mean fractions
 324 of MSA sub-type particles during leg I and leg II revealed that the uptake of MSA was affected by
 325 the particle chemical properties. Note that particle size also affects the uptake of MSA on fine
 326 particles. To clarify the uptake properties of MSA on different size particles, the size distributions
 327 of MSA particles (0.1-2.0 μm) and size-resolved MSA sub-type particles during leg I and leg II
 328 were also analyzed in this study. Although particles smaller than 0.1 μm were not detected by the
 329 SPAMS in this study, most of the MSA particles are in the range of 0.1 to 1.0 μm in the marine

330 atmosphere (Ayers et al., 1997), indicating that the MSA particles measured in this study represent
331 most of the MSA particles in the marine atmosphere.

332 The size of the total particles shows an unimodal distribution, with a mean diameter of 0.51 μm ,
333 during leg I and leg II (Fig. 5a). Most of the particles were in 0.3-1.0 μm , consisting with particle sizes
334 observed in Antarctica using SMPS (Pant et al., 2011), and with sea spray aerosol sizes measured in
335 marine regions (Quinn et al., 2017). Compare with mean size of the total particles, MSA particles
336 were larger in this study, with a mean diameter of 0.65 μm (Fig. 5a). This suggests that particles were
337 enlarged when MSA uptake occurred on their surfaces. Although particles were enlarged by MSA
338 uptake, submicron MSA particles contributed more than 90 % of the total MSA particles (Fig. 5b),
339 indicating that most of the MSA particles were still in the submicron range, consisting with observation
340 results in coastal Antarctica (Legrand et al., 1998) and the Pacific Ocean (Jung et al., 2014).

341 The size-resolved MSA sub-type particles by population fraction during leg I and leg II are also
342 given in this study. MSA-EC, MSA-K and MSA-NO_x⁻ particles were primarily distributed in small
343 size (<1 μm) (Fig. 5c). In contrast, high relative fractions of MSA-Na and MSA-Mg particles were
344 present in large particles (>1 μm), accounting for more than 75 % of the total coarse particles
345 (1.0~2.0 μm) (Fig. 5c). The relative fractions of MSA-SO₄²⁻ particles did not change significantly
346 as the particle size increases, mainly due to the variety sources of this type of particles. SO₄²⁻
347 particles are mainly derived from sea salt particles and the oxidation of DMS in the marine
348 atmosphere. Sea salt particles have a wide size distribution, ranging from 0.01-8 μm (Clarke et al.,
349 2006), which are found in submicron size (De Leeuw et al., 2011 and Prather et al., 2013) and
350 coarse size (Norris et al., 2013). But SO₄²⁻ particles generated from the oxidation of DMS are
351 mainly distributed in the submicron range (Legrand et al., 1998).

352 The MSA particle and total particle populations during leg II were much higher than during leg
 353 I (Fig. 5a) and seasonal conditions were different between leg I and leg II (Fig. S2), the
 354 size-resolved MSA sub-type particles identified during leg II were very similar with the
 355 size-resolved MSA sub-type particles identified during leg I (Fig. 5c and 5d), confirming the
 356 stable MSA uptake properties on different particles.



357
 358 Fig. 5 Size distributions of MSA particles and size-resolved MSA sub-type particles during the
 359 cruise, (a) Size distributions of MSA particles and total particles, (b) Cumulative size distributions
 360 of MSA and total particles, (c) Size-resolved MSA sub-type particles during leg I, and (d)
 361 Size-resolved MSA sub-type particles during leg II.

362 3.5. The uptake rate of MSA on different particles

363 The uptake of MSA on the existing particles has been investigated, however, the pressing
 364 question is how different aerosol properties impact the uptake rate of MSA. Fig. 6 shows the
 365 uptake rate of MSA (defined as the ratio of MSA-containing particles to the corresponding
 366 particles, such as MSA-Na to Na ratio) on different particles in marine atmosphere. The formation
 367 of particulate MSA includes two routes, the reactive uptake of DMS on existing aerosols, and the
 368 conversion of gaseous MSA to particulate MSA by condensation on existing particles (Read et al.,
 369 2008). High uptake rates of MSA-Na and MSA-Mg particles were observed in Na and Mg
 370 particles, accounting for 0.43 ± 0.21 and 0.41 ± 0.20 of the total Na and Mg particles,
 371 respectively (Fig. 6). There are two reasons for the effective uptake of MSA on Na and Mg

372 particles. Firstly, Na and Mg particles are mainly derived from sea salt particles, which are often
373 alkaline. Previous studies have shown that alkaline sea salt particles are favor to absorb acidic
374 atmospheric gases, promoting the formation of acidic compounds on sea salt particles (Laskin et
375 al., 2003). As an acidic species, MSA is easy to be absorbed by sea salt particles to form
376 particulate MSA. Secondly, the presence of halogen radicals on sea salt particle surfaces also
377 enhance the oxidative reactive uptake of DMS on those particles to form particulate MSA (Read et
378 al., 2008).

379 Low uptake rate (0.24 ± 0.68) of MSA-EC particles was observed in this study (Fig. 6).
380 Generally, EC particles are highly hydrophobic, which suppresses the uptake of MSA on these
381 particles, as DMS reactive uptake often occurs through aqueous reactions (Bardouki et al., 2003).
382 The relative fraction of SO_4^{2-} particles was much higher than that of EC particles (Fig. 4c).
383 However, the uptake rate of MSA- SO_4^{2-} particles (0.26 ± 0.47) was similar with that of
384 MSA-EC particles (Fig. 6), indicating that particle population was not the major factor affecting
385 MSA uptake rate. The uptake rate of MSA on existing particles is significant dependent on
386 particle characteristics. As SO_4^{2-} particles are often acidic, MSA uptake by this type of particle is
387 restricted. For this reason, even though SO_4^{2-} particle population was much higher than Na particle
388 population, the uptake rate of MSA- SO_4^{2-} particles was much lower than that of MSA-Na particles
389 (Fig. 6).

390 The uptake rates of MSA-OC and MSA- NO_x^- particles were 0.37 ± 0.38 and 0.35 ± 0.62 ,
391 respectively (Fig. 6). This is consistent with the relative abundances of MSA-OC and MSA- NO_x^-
392 particles and the corresponding OC and NO_x^- particles (Fig. 4). It indicates that the uptake rates of
393 MSA on existing particles were determined by the aerosol properties, alkaline sea salt particles
394 enhanced the uptake of MSA, while acidic and hydrophobicity species suppressed the uptake of
395 MSA on these particles.

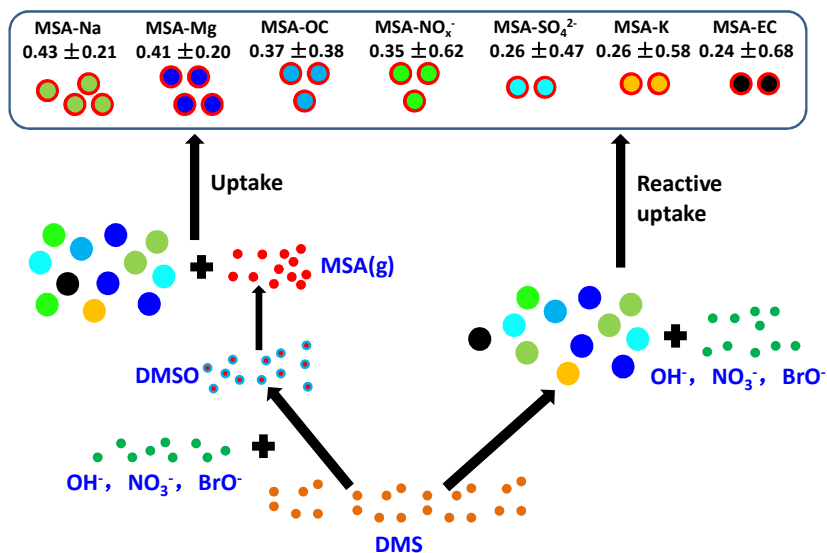


Fig. 6 MSA uptake rates on different aerosol particles in the marine atmosphere.

4. Conclusions

The uptake characteristics of MSA on different aerosols were examined during the early December 2017 and January-February 2018 in the polynya regions of the RS, Antarctica. Particulate MSA mass concentration, as well as particle populations and size distributions, were determined simultaneously for the first time to characterize the formation of MSA on different particles. To access the interactions between MSA and other species, MSA particles were classified into seven sub-types using the ART-2a algorithm: MSA-Na, MSA-Mg, MSA-SO₄²⁻, MSA-K, MSA-EC, MSA-OC, and MSA-NO_x⁻.

MSA mass concentration did not always reflect MSA particle population in the marine atmosphere. MSA uptake occurred on aerosol surfaces alters the aerosol size and chemical compositions, but did not change the aerosol population. MSA particle population was mainly associated with the total particle population, as more particles implies a greater opportunity for MSA uptake. High MSA mass concentrations with low MSA populations occurred, when low existing particle population with high MSA production from the oxidation of DMS were present.

The uptake of MSA on existing particles was mainly dependent on aerosol properties. Alkaline sea salt particles enhanced the uptake of MSA, as high uptake rates of MSA-Na and MSA-Mg particles were observed in the Na and Mg particles, accounting for 0.43 ± 0.21 and 0.41 ± 0.20 of

415 the total Na and Mg particles, respectively. But acidic and hydrophobicity species suppressed the
416 uptake of MSA on these particles, as only 0.24 ± 0.68 and 0.26 ± 0.47 of MSA-EC and
417 MSA-SO₄²⁻ were present in the total EC and SO₄²⁻ particles. The results extend the knowledge of
418 the impact of aerosol properties on the conversion of MSA in the marine atmosphere, however,
419 the details of the formation of MSA are complicated and still controversial. Observations and
420 especially simulation experiments in the laboratory are required in the future to clarify the
421 formation of MSA and their impact factors in the marine atmosphere.

422 **Code and Data availability.**

423 The data used in the figures, as well as the time series of the cruise tracks, MSA mass
424 concentration and particle mass concentrations obtained from the IGAC, MSA particle population,
425 size distribution and mass spectra obtained from the SPAMS, as well as wind speeds and
426 directions, temperature and RH, are available at <https://doi.org/10.5281/zenodo.3614694> (Jinpei
427 Yan, 2020). Codes for the analysis are available from JP upon request.

428 **Author contributions.**

429 JY conducted the observations, analyzed the results, and wrote the paper. JJ contributed the
430 data analyses and paper writing. MZ conducted the on-board observations. FB and YT contributed
431 to the refining the ideas and contributed considerably to the interpretation of the results. SX and
432 SZ applied the calculations of sea ice distribution and Metrological data. QL and LL contributed
433 the observation data analyses. LC and JY were together responsible for the design of the study. All
434 authors were involved in discussing the results and improved the paper by proofreading.

435 **Competing interests.**

436 The authors declare that they have no conflict of interest.

437 **Acknowledgements**

438 The authors gratefully acknowledge Guangzhou Hexin Analytical Instrument Company
439 Limited for the SPAMS data analysis and on-board observation technical assistance, and Zhangjia
440 Instrument Company Limited (Taiwan) for the IGAC technical assistance and data analysis. We
441 would like to thank Meijiao Pang for the SPAMS maintenance on-board during the cruise.

442 **Financial support**

443 This study is Financially Supported by Qingdao National Laboratory for marine science and
444 technology (No. QNLM2016ORP0109), the Natural Science Foundation of Fujian Province,
445 China (No. 2019J01120), the National Natural Science Foundation of China (No. 41941014).
446 Jinyoung Jung was supported by grants from Korea Polar Research Institute (KOPRI) (PE20140).

447 **References**

448 Adachi, K., Buseck, P. R. Changes in shape and composition of sea-salt particles upon aging in an urban
449 atmosphere. *Atmos. Environ.* 100, 1-9, 2015.

450 Allen, J.O. YAADA: Software Toolkit to Analyze Single-Particle Mass Spectral Data, 2005.

451 Ayers, G.P., Cainey, J.M., Gillett, R.W., Ivey, J.P. Atmospheric sulphur and cloud condensation nuclei in marine air
452 in the Southern Hemisphere, *Phil. Trans. R. Soc. Lond. B*, 352, 203-211, 1997.

453 Barnes, I., Hjorth, J., Mihalopoulos, N. Dimethyl sulfide and dimethyl sulfoxide and their oxidation in the
454 atmosphere. *Chem. Rev.* 106, 940-975, 2006

455 Bardouki, H., Berresheim, H., Erkoussis, M., Sciare, J., Kouvarakis, G., Oikonomou, K., Schneider, J.,
456 Mihalopoulos, N. Gaseous (DMS, MSA, SO₂, H₂SO₄ and DMSO) and particulate (sulphate and
457 methanesulfonate) sulphur species over the northeastern coast Crete. *Atmos. Chem. Phys.* 3, 1871-1886,
458 2003.

459 Bates, T. S., Calhoun, J. A., Quinn, P. K. Variations in the methane sulphonate to sulphate molar ratio in
460 submicrometer marine aerosol particles over the South Pacific Ocean. *J. Geophys. Res.* 97, 9859-9865, 1992.

461 Bork, N., Elm, J., Olenius, T., Vehkamäki. Methane sulfonic acid-enhanced formation of molecular clusters of
462 sulfuric acid and dimethyl amine. *Atmos. Chem. Phys.* 14, 12023-12030, 2014.

463 Casillas-Ituarte, N.N., Callahan, K. M., Tang, C.Y., Chen, X., Roeselova, M. Surface organization of aqueous
464 MgCl₂ and application to atmospheric marine aerosol chemistry. *PNAS*, 107, 6616-6621, 2010.

465 Cavalieri, D. J., and Parkinson, C. L. 30-Year satellite record reveals contrasting Arctic and Antarctic decadal sea
466 ice variability. *Geophys. Res. Lett.* 30(18), 2003.

467 Chang, R. Y.-W., Sjostedt, S. J., Pierce, J. R., Papakyriakou, T. N., Scarratt, M. G., Michaud, S., et al. Relating
468 atmospheric and oceanic DMS levels to particle nucleation events in the Canadian Arctic. *J. Geophys. Res.*
469 116, D00S03, 2011.

470 Chen, L., Wang, J., Gao, Y., Xu, G., Yang, X., Lin, Q., Zhang, Y. Latitudinal distributions of atmospheric MSA and
471 MSA/nss-SO₄²⁻ ratios in summer over the high latitude regions of the Southern and Northern Hemispheres. *J.*
472 *Geophys. Res.* 117, D10306, 2012.

473 Clarke, A. D., Owens, S. R. Zhou, J. An ultrafine sea-salt flux from breaking waves: implications for cloud
474 condensation nuclei in the remote marine atmosphere. *J. Geophys. Res.* 111, D06202.
475 (doi:10.1029/2005JD006565), 2006.

476 Davis, D., Chen, G., Kasibhatla, P., Jefferson, A., Tanner, D., Eisele, F., Lenschow, D., Neff, W., Berresheim, H.
477 DMS oxidation in the Antarctic marine boundary layer: Comparison of model simulations and field
478 observations of DMS, DMSO, DMSO₂, H₂SO₄(_g), MSA(_g), and MSA(_p). *J. Geophys. Res.* 103, 1657-1678,
479 1998.

480 De Baar, H. J., De Jong, J. T., Bakker, D. C., Löscher, B. M., Veth, C., Bathmann, U., Smetacek, V. Importance of
481 iron for plankton blooms and carbon dioxide drawdown in the Southern Ocean. *Nature*, 373, 412-415, 1995.

482 De Leeuw, G., Andreas, E. L., Anguelova, M. D., Fairall, C. W., Lewis, E. R., O'Dowd, C., Schulz, M., and
483 Schwartz, S. E. Production flux of sea spray aerosol, *Rev Geophys.*, 49, RG2001,
484 doi:10.1029/2010RG000349, 2011.

485 Gaston, C.J., Furutani, H., Guazzotti, S. A., Coffee, K.R., Bates, T.S., Quinn, P.K., Aluwihare, L.I. Mitchell, B.G.,
486 Prather, K. Unique ocean-derived particles serve as a proxy for changed in ocean chemistry. *Journal of*
487 *Geophysical Research*, 116, D18310, 2011

488 Guazzotti, S. A., Coffee, K. R., Prather K. A. Continuous measurements of size - resolved particle chemistry

489 during INDOEX Intensive Field Phase 99, *J. Geophys. Res.*, 106(D22), 28,607 - 28,627,
490 doi:10.1029/2001JD900099, 2001.

491 Ghahremaninezhad, R., Norman, A.-L., Abbatt, J. P. D., Levasseur, M., Thomas, J. L. Biogenic, anthropogenic and
492 sea salt sulfate size-segregated aerosols in the Arctic summer. *Atmos. Chem. Phys.* 16, 5191-5202, 2016.

493 Hayashida, H., Steiner, N., Monahan, A., Galindo, V., Lizotte, M., Levasseur, M. Implications of sea-ice
494 biogeochemistry for oceanic production and emissions of dimethyl sulfide in the Arctic. *Biogeosciences*. 14,
495 3129-3155, 2017.

496 Healy, R. M., Hellebust, S., Kourtchev, I., Allanic, A., O'Connor, I. P., Bell, J. M., Healy, D. A., Sodeau, J. R.,
497 Wenger, J. C. Source apportionment of PM_{2.5} in Cork Harbour, Ireland using a combination of single particle
498 mass spectrometry and quantitative semi-continuous measurements. *Atmos. Chem. Phys.* 10, 9593-9613, 2010.

499 Horne, J.R., Zhu, S., Montoya-Aguilera, J., Hinks, M.L., Wingen, L.M., Nizkorodov, S.A., Dabdub, D. Reactive
500 uptake of ammonia by secondary organic aerosols: Implications for air quality. *Atmos. Environ.* 189, 1-8,
501 2018.

502 Jung, J., Furutani, H., Uematsu, M., Park, J.. Distributions of atmospheric non-sea-salt sulfate and methanesulfonic
503 acid over the Pacific Ocean between 48°N and 55°S during summer. *Atmos. Environ.* 99, 374-384, 2014.

504 Kloster, S., Feichter, J., Maier-Reimer, E., Six, K. D., Stier, P., Wetzzel, P. DMS cycle in the marine
505 ocean-atmosphere system? a global model study. *Biogeosciences*, 3, 29-51, 2006.

506 Laskin, A., Gaspar, D.J., Wang, W., Hunt, S. W., Cowin, J.P., Colson, S.D., Finlayson-Pitts, B.J. Reactions at
507 interfaces as a source of sulfate formation in sea-salt particles. *Science*, 301(5631), 340-344, 2003.

508 Legrand, M., Pasteur, E. C. Methane sulfonic acid to non-sea-salt sulfate ratio in coastal Antarctic aerosol and
509 surface snow. *J. Geophys. Res.* 103, 10991-11006, 1998.

510 Li, L., Huang, Z., Dong, J., Li, M., Gao, W., Nian, H., Fu, Z., Zhang, G., Bi, X., Cheng, P., Zhou, Z. Real time

511 bipolar time-of-flight mass spectrometer for analyzing single aerosol particles. *Int. J. Mass Spectrom.* 303,
512 118-124, 2011.

513 Li, L., Li, M., Huang, Z.X., Gao, W., Nian, H.Q., Fu, Z., Gao, J., Chai, F.H., Zhou, Z. Ambient particle
514 characterization by single particle aerosol mass spectrometry in an urban area of Beijing. *Atmos. Environ.* 94,
515 323-331, 2014.

516 Liu, M., Song, Y., Zhou, T., Xu, Z., Yan, C., Zheng, M., Wu, Z., Hu, M., Wu, Y., Zhu, T. Fine particle pH during
517 severe haze episodes in northern China, *Geophys. Res. Lett.* 44, 5213-5221, 2017.

518 Lizotte, M. P. The Contributions of Sea Ice Algae to Antarctic Marine Primary Production. *Am. Zool.* 41, 57-73,
519 2001.

520 Loose, B., Miller, L. A., Elliott, S., Papakyriakou, T. Sea ice biogeochemistry and material transport across the
521 frozen interface. *Oceanography*, 24, 202-218, 2011.

522 Mazzer, D. M., Lowenthal, D. H., Chow, J. C., Watson, J. G. Sources of PM₁₀ and sulfate aerosol at McMurdo
523 Station, Antarctica. *Chemosphere*, 45, 347-356, 2001.

524 Minikin, A., Legrand, M., Hall, J., Wagenbach, D., Kleefeld, C., Wolff, E., Pasteur, E. C., Ducroz, F.
525 Sulfur-containing species (sulfate and methanesulfonate) in coastal Antarctic aerosol and precipitation, *J.*
526 *Geophys. Res.*, 103, 10975-10990, 1998.

527 Murphy, S. M., Agrawal, H., Sorooshian, A., Padró, L.T., Gates, H., Hersey, S. Comprehensive simultaneous
528 shipboard and airborne characterization of exhaust from a modern container ship at sea. *Environ. Sci. Tech.*
529 43, 4626-4640, 2009.

530 Norris, S. J., Brooks, I. M., Moat, B. I., Yelland, M. J. Near-surface measurement of sea spray aerosol production
531 over whitecaps in the open ocean. *Ocean Sci.* 9, 133-145, 2013.

532 Pant, V., Singh, D., Kamra, A.K., Size distribution of atmospheric aerosols at Maitri, Antarctica. *Atmospheric*

533 Environment, 45, 5138-5149, 2011.

534 Prather, K.A., Bertram T.H., Grassian V.H., Deane G.B., Stokes M.D., DeMott P.J., Aluwihare L.I., Palenik B.P.,
535 Azam, F. Seinfeld J.H., Moffet, R.C., Molina, M.J., Cappa, C.D., Geiger, F.M., Roberts, G.C., Russell, L.M.,
536 Ault, A.P., Baltrusaitis, J., Collins, D.B., Corrigan, C.E., Cuadra-Rodriguez, L.A., Ebben, C.J., Forestieri, S.D.,
537 Guasco, T.L., Hersey, S.P., Kim, M.J., Lambert, W.F., Modini, R.L., Mui, W., Pedler, B.E., Ruppel, M.J.,
538 Ryder, O.S., Schoepp, N.G., Sullivan, R.C., Zhao D. Bringing the ocean into the laboratory to probe the
539 chemical complexity of sea spray aerosol. PNAS, 110(19):7550-7555, 2013.

540 Preunkert, S., Jourdain, B., Legrand, M., Udisti, R., Becagli, S., Cerri, O. Seasonality of sulfur species (dimethyl
541 sulfide, sulfate, and methanesulfonate) in Antarctica: Inland versus coastal regions. J. Geophys. Res. 113,
542 D15302, 2008.

543 Preunkert, S., Legrand, M., Jourdain, B., Moulin, C., Belviso, S., Kasamatsu, N., Fukuchi, M., Hirawake, T.
544 Interannual variability of dimethylsulfide in air and seawater and its atmospheric oxidation by-products
545 (methanesulfonate and sulphate) at Dumont d'Urville, coastal Antarctica (1999-2003). J. Geophys. Res. 112,
546 2007.

547 Quinn, P.K., Coffman, D.J., Johnson, J.E., Upchurch, L.M., Bates, T.S. Small fraction of marine cloud
548 condensation nuclei made up of sea spray aerosol, Nature Geoscience, doi:10.1038/NGEO3003, 2017.

549 Quinn, P.K., Bates, T.S., Schulz, K.S., Coffman, D.J., Frossard, A.A., Russell, L.M., Keene, W.C., Kieber, D.J.
550 Contribution of sea surface carbon pool to organic matter enrichment in sea spray aerosol. Nature Geos. 7,
551 228-232, 2014.

552 Read, K. A., Lewis, A. C., Bauguutte, S., Rankin, A. M., Salmon, R. A., Wolff, E. W., Saiz-Lopez, A., Bloss W. J.,
553 Heard, D. E., Lee, J. D., Plane, J. M. C. DMS and MSA measurements in the Antarctic Boundary Layer:
554 impact of BrO on MSA production. Atmos. Chem. Phys. 8, 2985-2997, 2008.

555 Savoie, D.L., Prospero, J.M., Larsen, R.J., Huang, F., Izaguirre, M.A., Huang, T., Snowdon, T.H., Custals, L.,
556 Sanderson, C.G. Nitrogen and sulfur species in Antarctic aerosols at Mawson, Palmer, and Marsh (King
557 George Island), *J. Atmos. Chem.* 17, 95-122, 1993.

558 Schlitzer, R. Ocean Data View, *Odv.awi.de*, 2015.

559 Schlitzer, R. Interactive analysis and visualization of geosciences data with Ocean Data view. *Comput. Geosci.* 28,
560 1211-1218, 2002.

561 Song, X.H., Hopke, P.K., Fergenson, D.P., Prather, K.A. Classification of single particles analyzed by ATOFMS
562 using an artificial neural network, *ART-2A. Analy. Chem.* 71, 860-865, 1999.

563 Sorooshian, A., Lu, M. L., Brechtel, F. J., Jonsson, H., Feingold, G., Flagan, R.C., Seinfeld, J.H. On the source of
564 organic acid aerosol layers above clouds. *Environ. Sci. Technol.* 41, 4647-4654, 2007.

565 Spreen, G., Kaleschke, L., and Heygster, G. Sea ice remote sensing using AMSR-E 89 GHz channels, *J. Geophys.*
566 *Res.*, 113, C02S03, 2008.

567 Silva, P. J., Carlin, R. A., Prather, K. A. Single particles analysis of suspended soil dust from Southern California.
568 *Atmos. Environ.* 34, 1811-1820, 2000.

569 Sitaras, I. E., Siskos, P. A. The role of primary and secondary air pollutants in atmospheric pollution: Athens urban
570 area as a case study. *Environ. Chem. Lett.* 6, 59-69, 2008.

571 Tao, J., Zhang, Z., Tan, H., Zhang, L., Wud, Y., Sun, J., Chee, H., Cao, J., Cheng, P., Chen, L., Zhang, R.
572 Observation evidence of cloud processes contributing to daytime elevated nitrate in an urban atmosphere.
573 *Atmos. Environ.* 186, 209-215, 2018.

574 Taylor, M. H., Losch, M., Bracher, A. On the drivers of phytoplankton blooms in the Antarctic marginal ice zone:
575 A modeling approach. *J. Geophys. Res.* 118, 63-75, 2013.

576 Teinila, K., Frey, A., Hillamo, R., Tulp, H. C., Weller, R. A study of the sea-salt chemistry using size-segregated

577 aerosol measurements at coastal Antarctic station Neumayer. *Atmos. Environ.* 96, 11-19, 2014.

578 Tian, M., Wang, H., Chen, Y., Zhang, L., Shi, G., Liu, Y., Yu, J., Zhai, C., Wang, J., Yang, F. Highly time-resolved
579 characterization of water-soluble inorganic ions in PM_{2.5} in a humid and acidic mega city in Sichuan Basin,
580 China. *Sci. Total Environ.* 580, 224-234, 2017.

581 Wang, S., Bailey, D., Lindsay, K., Moore, J. K., Holland, M. Impact of sea ice on the marine iron cycle and
582 phytoplankton productivity. *Biogeosciences*, 11, 4713-4731, 2014.

583 Weller, R., Legrand, M., Preunkert, S. Size distribution and ionic composition of marine summer aerosol at the
584 continental Antarctic site Kohnen. *Atmos. Chem. Phys.*, 18, 2413-2430, 2018.

585 Wolff, E. Nitrate in polar ice, in *Ice Core Studies of Global Biogeochemical Cycles*, edited by R. Delmas,
586 Springer-Verlag, New York, 195-224, 1995.

587 Yan, J., Lin, Q., Zhao, S., Chen, L., Li, L. Impact of marine and continental sources on aerosol characteristics
588 using an on-board SPAMS over Southeast Sea, China. *Environ. Sci. Pollution Res.* 25, 30659-30670, 2018.

589 Yan, J., Chen, L., Lin, Q., Li, Z., Chen, H., Zhao, S. Chemical characteristics of submicron aerosol particles during
590 a long-lasting haze episode in Xiamen, China. *Atmos. Environ.* 113, 118-126, 2015.

591 Young, L. H., Li, C. H., Lin, M. Y., Hwang, B. F., Hsu, H. T., Chen, Y. C., Jung, C. R., Chen, K. C., Cheng, D. H.,
592 Wang, V. S., Chiang, H. C., Tsai, P. J. Field performance of semi-continuous monitor for ambient PM_{2.5}
593 water-soluble inorganic ions and gases at a suburban site. *Atmos. Environ.* 144,376-388, 2016.

594 Zhang, M., Chen, L., Xu, G., Lin, Q., Liang, M. Linking phytoplankton activity in polynyas and sulfur aerosols
595 over Zhongshan Station, East Antarctica. *J. Atmos. Sci.* 72, 4629-4642, 2015.